Raman scattering and attenuated-total-reflection studies of surface-plasmon polaritons

K. Kurosawa,* R. M. Pierce, and S. Ushioda†
Department of Physics, University of California, Irvine, California 92717

J. C. Hemminger
Department of Chemistry, University of California, Irvine, California 92717
(Received 30 August 1985)

We have made *in situ* measurements of attenuated total reflection (ATR) and Raman scattering from a layered structure consisting of a glass prism, a thin silver film, an MgF_2 spacer, and a liquid mixture whose refractive index is matched to that of MgF_2. When the incident angle of the laser beam coincides with the ATR angle, the surface-plasmon polariton (SPP) of the silver film is excited resonantly and the Raman scattering intensity of the liquid shows a maximum. The same effect is observed at the frequency of the Stokes scattered light. By measuring the decrease of the Raman scattering intensity of the liquid with increase of the thickness of the MgF_2 spacer layer, we have determined the decay length (l_d) of the SPP field into the liquid. The measured value of $l_d = 1539$ Å agrees with the calculated value, 1534 Å.

I. INTRODUCTION

When an incident beam of light, which is a volume electromagnetic wave (VEW), is injected into a surface electromagnetic wave (SEW), such as surface-plasmon polaritons (SPP's), the resultant amplitude of the electromagnetic (EM) fields at the surface can be many times greater than that of the incident wave. The theory of this effect is well understood,[1,2] and also, experimentally, the effect has been utilized to study various physical phenomena near the interfaces between metals and dielectrics.[3–6]

Ushioda and Sasaki[3] used the Kretschmann configuration, which consists of a glass prism, a thin silver film, and a liquid (methanol) in contact with the silver film. The exciting laser beam was injected into the SPP's of silver through the prism and the scattered light was collected again through the prism. They measured the Raman scattering intensity of the 2835-cm^{-1} line of methanol as a function of the incident and of the scattering angle, and found that the Raman scattering intensity has a maximum when either the incident angle or the scattering angle satisfies the optimum resonant excitation condition of SPP's. In that work the penetration depth or the decay length (l_d) of the EM field of SPP's into the liquid was estimated from theory to be 1400 Å.

In the present work we have actually measured the decay length of the EM field in the liquid. A spacer layer of different thicknesses of MgF_2 was evaporated on top of the silver film to lie between the silver film and the liquid. Then the Raman scattering intensity of the liquid (acetone) was measured for different thicknesses of the spacer layer. By mixing a small amount of nitrobenzene in acetone, the refractive index of the liquid was matched to that of MgF_2; thus, optically, there is no interface between MgF_2 and the liquid, and therefore the decay of the SPP field outside the silver film behaves exactly as if the liquid is in direct contact with the silver film. Then a logarithmic plot of the Raman intensity from acetone versus the spacer thickness gives the decay constant of SPP's in the liquid.

Furthermore, we have measured the angle dependence of the Raman intensity and the attenuated-total-reflection (ATR) spectra of a single sample *in situ*, so that the relation between the excitation of SPP's and the enhanced Raman intensity can be clearly seen.

II. THEORY

Most of the necessary theoretical tools for analysis of the data are developed in the Appendix. We will use two formulas presented there, for reflectivity R and transmissivity T, Eq. (A17) and Eq. (A19), respectively. Our sample system consists of four layers; media 1–4 correspond to a liquid, MgF_2, Ag, and a glass prism, as indicated in Fig. 1. Thus, $n = 4$ in Eq. (A19). The reflectivity measured in ATR experiments is given by Eq. (A17). The intensity of the incident light at the silver-MgF_2 interface is obtained by Eq. (A19) as a function of the incident angle.

Since $M_{22} = 0$ corresponds to the dispersion relation of

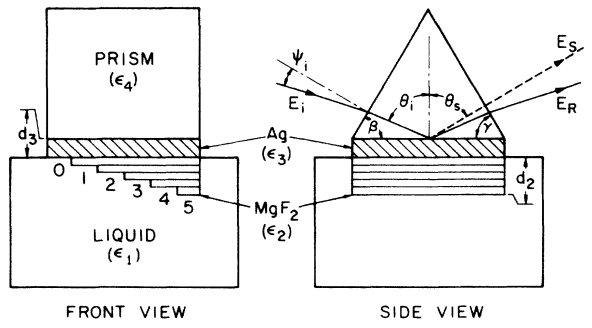

FIG. 1. Geometry of the sample system. The six regions of different MgF_2 spacer thicknesses are indicated by 0–5.

SPP's, the transmissivity T has a peak when $(k_{||},\omega)$ nearly satisfies the dispersion relation. For real ω, $M_{22}=0$ is realized only for complex $k_{||}$, which means that SPP's decay along the surface. Since in actual experiments $k_{||}$ is always real, M_{22} never becomes zero, but becomes small when θ_i is such that $(k_{||},\omega)$ is near the true zero of M_{22} in the complex plane. Consequently, T has a finite maximum on the real $k_{||}$ axis for a fixed real ω.

Next, let us examine the behavior of the reflectivity R. Since M_{22} appears in the denominator of Eq. (A17) for R, one might casually think that R should have a maximum near the zero of M_{22}. However, actual numerical calculations show that $|M_{12}|$ in the numerator has a strong minimum at a value of $k_{||}$(real) for which $|M_{22}|$ is nearly zero. Thus the net result is that R has a sharp minimum very close to but not exactly at the point where the dispersion relation for SPP's is satisfied by $(k_{||},\omega)$. Because of this fairly delicate balance between $|M_{12}|$ and $|M_{22}|$, the minimum of R and the maximum of T almost coincide at the value of $k_{||}$(real) which corresponds to the dispersion curve of SPP's.

From Eq. (A19) we know the intensity of the incident laser light at the site of the scattering molecules, i.e., at the silver-liquid or the MgF_2-liquid interface. The scattered light is emitted by the induced dipole of the vibrating molecules, so we need to know how the dipole radiation with its source located at the bottom of the stack is propagated into the prism at the top. It can be shown[7] that the same expression as Eq. (A19) applies to this reverse propagation process for the scattered light with $\omega=\omega_s$ (Raman-scattered frequency) and $\theta=\theta_s$ (scattering angle with respect to the surface normal). To distinguish the incident- and scattered-light parameters, we define $T(\omega_i,\theta_i)$ and $T(\omega_s,\theta_s)$, which stand for the expressions of Eq. (A19) with the appropriate frequencies and angles substituted for ω and θ. We also define wave-vector components $k_z(1,\omega_i)$ and $k_z(1,\omega_s)$ at the incident and scattered frequencies given by Eq. (A3). Then the Raman-scattered intensity in the prism can be written in the form

$$I(\theta_i,\theta_s,d_2)=AT(\omega_i,\theta_i)T(\omega_s,\theta_s)\times\exp\{2i[k_z(1,\omega_i)+k_z(1,\omega_s)]d_2\}\ , \quad (1)$$

where d_2 is the thickness of the MgF_2 spacer layer and A is a constant. For the range of angles of interest here, that is, θ_i, $\theta_s>\theta_c$, where $\sin\theta_c=(\epsilon_1/\epsilon_4)^{1/2}$, $k_z(1,\omega_i)$ and $k_z(1,\omega_s)$ are pure imaginary and $\mathrm{Im}k_z(1,\omega_i)$ and $\mathrm{Im}k_z(1,\omega_s)$ are positive. Thus $I(\theta_i,\theta_s,d_2)$ decreases with increasing spacer thickness d_2. We will measure the Raman intensity $I(\theta_i,\theta_s,d_2)$ as a function of d_2 and determine the value of $2i[k_z(1,\omega_i)+k_z(1,\omega_s)]^{-1}$, which is the penetration distance of the SPP's into the liquid.

III. EXPERIMENT

A. Experimental setup

The experimental setup that can perform both ATR spectroscopy and Raman spectroscopy on a single sample system *in situ* is sketched in Fig. 2. For Raman scattering the 5145-Å line of an argon-ion laser was used as the incident light, and for ATR measurements the same argon-ion-laser line as well as a dye-laser line at 6059 Å was used. The latter wavelength corresponds to the Stokes-scattered Raman emission from the 2930-cm^{-1} line of acetone.

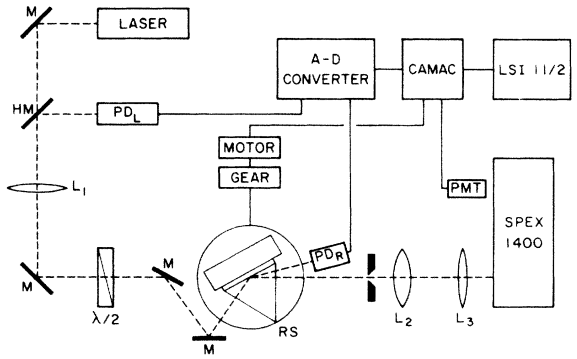

FIG. 2. Optical setup to measure ATR and Raman scattering on a single sample system *in situ*.

The ATR setup requires a precision rotation and detection system. It consists of three parts, a prism and cell, a motor-driven rotation stage, and a detection system. The prism is an ordinary spectrographic dispersion prism (Schott F2 glass). The silvered side is pressed onto a Teflon O-ring seal fixed to the sample cell. The sample cell is also made of Teflon to allow for use of a wide variety of liquids. The prism-cell is mounted to an in-line, driven rotation stage whose rotation axis is in the horizontal plane. The rotation stage is driven by a stepping motor and a precision speed reducer providing a total of 200 steps/deg rotation. Both the drive system and the rotation stage are supported on an optical bench, allowing continuous translation of the rotation system or easy decoupling of the rotation stage from the drive. Additional degrees of freedom are provided by a small, high-precision goniometer fixed to the rotation stage, which, in turn, supports the prism-cell. The goniometer gives two translations and two rotations orthogonal to those just mentioned. These combine to allow accurate positioning of the prism into the path of the incident laser beam.

The detection system consists of two photodiodes, one for detection of the incident-laser-beam intensity (PD_L) and the other for measurement of the reflected beam (PD_R). The reflected intensity is measured with a large-area photodiode (7.6×5.6 mm^2) which is fixed directly to the rotation stage. This arrangement eliminates the need for a separate 2θ scan for the diode (which must follow the θ scan of the prism). In combination with the large-area photodiode, this method can give as much as a 30-deg scanning range for a single scan. Both diodes are monitored by an analog-to-digital (A/D) converter controlled by a CAMAC (computer-aided measurement and control) data-acquisition system, which is, in turn, interfaced to a Digital Equipment Corporation LSI-11/2 minicomputer. The computer system also runs the stepping motor for the rotation stage and calculates appropriate conversion of external angles (ψ_i) of incidence to angles

(θ_i) of incidence inside the triangular prism using the following equation:

$$\psi_i = \sin^{-1}[(\epsilon_4)^{1/2}\sin(\theta_i - \beta)] , \quad (2)$$

where β is one of the apex angles of the prism (see Fig. 1). The rotation system is aligned by observing the laser beam reflected from one of the flat faces of the prism and setting the reflection angle to zero. Such a method gives an accuracy of better than ± 0.05 deg, which complements the short-scan scanning precision of ± 0.01 deg. These uncertainties have been determined by performing a total-internal-reflection scan with a prism of known index of refraction.

Raman scattering measurements were made using a Spex Industries 1400 double-grating spectrometer controlled by the CAMAC–LSI-11/2 system that also controls the ATR setup as described before. Since this part of the measurement system has been described in previous publications, no further discussion will be given. To measure the Raman intensity as a function of the incident angle, the laser beam with the convergence angle of 0.05 deg was kept fixed, while the prism was rotated. For measurements of the scattering-angle dependence of the Raman intensity, a rectangular slit of 1×5 mm^2 was placed 10 cm from the silvered surface and its lateral position was varied to change the scattering angle. Using this method, the angular accuracy is about 0.1 deg and the range of the scattering angle collected is 0.5 deg.

B. Sample preparation

As shown in Fig. 1, the sample system consists of a triangular glass prism (Schott F2 glass), an evaporated silver film, a stepped evaporated film of MgF_2, and a liquid in contact with the film surface. After cleaning the prism surface, a silver film was evaporated on it at an evaporation rate of about 2 Å/s. Subsequently, a MgF_2 film was evaporated over the silver film in successive steps to create regions of different thicknesses. The film thicknesses were monitored by a quartz oscillator gauge.

The apex angles (β and γ in Fig. 1) were determined by shining a laser beam onto the flat prism faces and rotating the prism until the backreflected beam coincides with the incident beam. Their values were $\beta = 60.040 \pm 0.005$ deg and $\gamma = 59.850 \pm 0.005$ deg. The refractive index of the prism was determined from the total-internal-reflection (TIR) angle of the 5145-Å line of an argon-ion laser at the prism-air interface. The refractive index thus obtained agrees within the experimental uncertainty with the value given in a data sheet of Schott Glass Company; therefore, we have used the refractive-index data provided by the manufacturer for all wavelengths. Using the known apex angles and the refractive index of the prism, the refractive index of the liquid was determined by measuring the TIR angle at the prism-liquid interface. The liquid used in this experiment was prepared by mixing acetone ($n = 1.36$) and nitrobenzene ($n = 1.56$). The refractive index was adjusted by adding nitrobenzene to acetone by titration until it matched that of MgF_2 [$(\epsilon_2)^{1/2} = 1.37$]. This index matching was further checked by comparing the ATR spectra of Region 0 of Fig. 1, where there is no MgF_2 coating, and other regions coated by MgF_2. When the index matching is accomplished, the ATR spectra of these regions were identical, because MgF_2 and the mixture are optically identical. The index-matched mixture consists of about 10 vol % of nitrobenzene in acetone.

The precise thickness and the dielectric constant (complex) of the silver film was determined by fitting the ATR curve to the exact reflectivity formula given by Eq. (A17). Then the thickness and dielectric constant of MgF_2 could be found by using the known data for silver and a similar fitting procedure.

C. ATR measurements

Figure 3 shows the ATR curves of the sample shown in Fig. 1 taken with the incident light at 5145 Å. Each numbered curve was obtained for the corresponding region of the sample numbered 0–5 having different thicknesses of the MgF_2 overcoating. The liquid cell was empty for these measurements. We note that the width of the resonance broadens with increasing thickness of the MgF_2 coating and, at the same time, the position of the ATR dip shifts to larger angles. On the other hand, the depth of the dip remains constant. From these curves both the thicknesses and the dielectric constant of the MgF_2 overcoating can be determined by curve fitting. However, before we deal with the thickness of the overcoating we must carefully consider the characteristics of the silver film first.

By fitting curve 0 for the bare silver film in contact with air, we can determine the dielectric constant (ϵ_3) and the thickness (d_3) of the silver film. Using the refractive index of the prism, $\epsilon_4 = 2.650$, we obtain $\epsilon_3 = -9.39 + i\,0.39$ and $d_3 = 619$ Å. These values are for the exposed portion of the silver film, and as we see below they differ from the corresponding values obtained for the coated portion of the film.

When the cell is filled with the index-matched mixture of acetone and nitrobenzene, the ATR curves obtained from all the regions (regions 0–5) are identical, and for

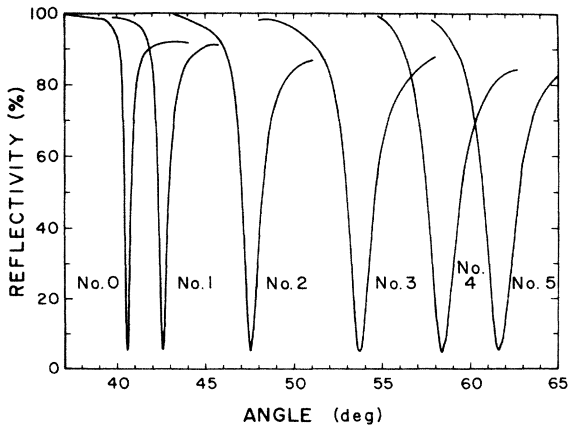

FIG. 3. ATR spectra of the six different sample regions with no liquid in the cell.

clarity we show only one set of such data points by the solid circles in Fig. 4. This result shows that index matching between MgF_2 and the liquid mixture has been accomplished successfully, and the whole medium below the silver-MgF_2 interface looks uniform to SPP's excited at the silver surface. The solid curve of Fig. 4 represents the best least-squares fit of the data to Eq. (A17), using the dielectric constants of the prism ($\epsilon_4=2.650$) and MgF_2 and the liquid ($\epsilon_1=\epsilon_2=1.870$). From this curve we obtain the parameters of the silver film: $\epsilon_3=-10.19+i0.414$ and $d_3=589$ Å. Note that the thickness of the MgF_2 film does not enter the fitting procedure here because its refractive index is identical to that of the liquid.

We notice that these values of the parameters of the silver film are different from the ones obtained from curve 0 of Fig. 3. Since the silver film was evaporated everywhere all at once, we expected to find identical values for these parameters. As far as region 0 is concerned, the only difference in the two measurement procedures is whether the silver film is in contact with air or with the liquid. Other regions of the film are in contact with MgF_2 in both measurements. Apparently, contact with a liquid or MgF_2 affects the dielectric behavior of the silver film. This effect was observed previously by Gugger *et al.*[8] In this connection the data set shown by open squares in Fig. 4 are very interesting. This ATR curve was obtained from the uncoated region (region 0) after exposure to the laser light while in contact with the liquid, i.e., after Raman measurements. We see that substantial change has occurred to the uncoated film during exposure. On the other hand, the ATR curves of the coated regions, even after Raman experiments, were identical to the data set represented by the solid circles, that is, no change occurred after extended exposure to laser light. If we assume that the dielectric constant of the unaffected portion of the silver film is given by $\epsilon_3=-10.19+i0.414$, to fit the data of the open squares we must assume the presence of an overlayer of thickness $d_{0l}=130$ Å and the dielectric constant $\epsilon_{0l}=-9.0+i1.1$. For this

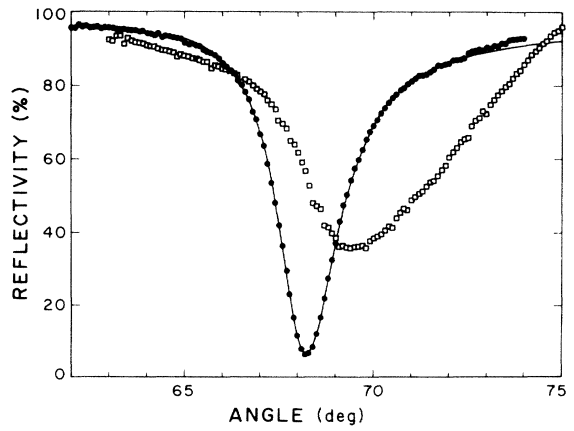

FIG. 4. ATR spectrum with the cell field with the index-matched liquid. Solid circles: before extended laser exposure for all regions. Open squares: bare Ag (region 0) after extended laser exposure. Solid curve: best fit with $\epsilon_3=-10.19+i0.414$ and $d_3=589$ Å.

fit the thickness of the unaffected portion of the silver film was $d_3=438$ Å. This result indicates that the uncoated silver surface is oxidized or otherwise affected by exposure to air, liquid, and laser radiation, while the MgF_2 film protects the coated portion of the silver surface. The thickness and dielectric constant of the overlayer obtained by the above fitting procedure appear reasonable. We also want to mention here that the ATR curves change with time if the incident laser power is greater than about 30 mW. With increasing exposure the dip position moves toward smaller angles and the dip width broadens. This kind of change is not observed in the coated regions with an MgF_2 thickness of more than 100 Å. Apparently, external atoms and molecules can diffuse through about 100 Å of MgF_2.

Now, returning our attention to curve 0 of Fig. 3, we have tried to fit this curve assuming the presence of an overlayer between silver and air. We found that for the best fit we need to assume an overlayer of thickness 10 Å and dielectric constant 3.0. With this assumption, the silver-film parameters of $\epsilon_3=-10.19+i0.414$ and $d_3=589$ Å give a very good fit. This result suggests that whatever happens at the silver-dielectric interface, it affects only a very thin layer near the interface.

From these detailed considerations, we have decided that the appropriate values of the parameters to use for the silver film are $\epsilon_3=-10.19(\pm0.02)+i0.414(\pm0.005)$ and $d_3=589\pm17$ Å. Using these parameter values, the thicknesses of the MgF_2 film for the different regions were determined by least-squares fitting of the ATR curves in Fig. 3. These thicknesses are listed in Table I. We will use these values in the following Raman scattering experiment.

D. Raman scattering

Using the Raman scattering technique, we have carried out two kinds of experiments. In the first part the Raman intensity from the 2930-cm^{-1} line of acetone was measured as a function of both incident and scattering angles, and the angle dependence of the Raman intensity was compared with the ATR intensity. This experiment definitively confirms the result by Ushioda and Sasaki[3] that the Raman-intensity change with angles is due to resonance excitation of SPP's. In the second part the Raman intensity of the same vibration line of acetone was measured as a function of the thickness of the MgF_2 spacer layer. By this experiment we were able to determine the

TABLE I. Thickness of MgF_2 spacers for different sample regions.

Region no.	MgF_2 thickness d_2 (Å)
0	0
1	142±2
2	374±2
3	611±2
4	817±2
5	1003±2

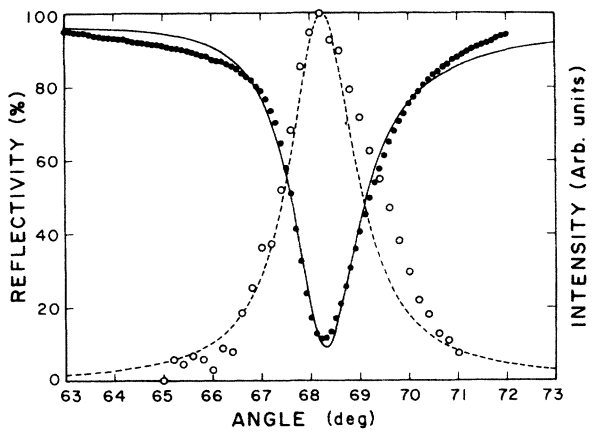

FIG. 5. Open circles: Raman intensity as a function of the incident angle. Solid circles: ATR spectrum at 5145 Å. Solid curve: best fit for ATR data. Dashed curve: Raman intensity calculated from Eq. (A19) using the best-fit parameters from the ATR curve.

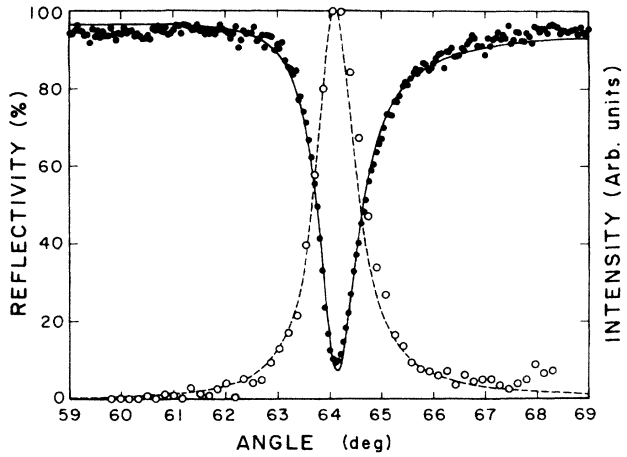

FIG. 6. Open circles: Raman intensity as a function of the scattering angle. Solid circles: ATR spectrum at 6059 Å. Solid curve: best fit for ATR data. Dashed curve: Raman intensity calculated from Eq. (A19) using the best-fit parameters from the ATR data.

decay length or the penetration depth (l_d) of the SPP field outside the silver film.

The open circles in Fig. 5 show the incident-angle dependence of the Raman intensity of the 2930-cm^{-1} line of acetone taken with the 5145-Å line of an argon-ion laser as the exciting source. The sample consists of about 600 Å of silver and 100 Å of MgF_2 overcoating in contact with the index-matched liquid described before. The p-polarized exciting beam was incident on the prism-Ag interface from the prism side, and the incident angle was measured from the surface normal inside the prism. While the incident angle was varied, the scattering angle was kept fixed at about 64 deg, where the scattered light has a resonance, as we see later in Fig. 6. The solid circles in Fig. 5 represent the ATR intensity measured at the same spot on the silver film using the same laser line. We see that the position of the maximum Raman intensity exactly coincides with the ATR dip position. This demonstrates that the maximum in the Raman intensity occurs when an SPP is excited resonantly by the incident light.

The solid curve represents the best least-squares fit for the ATR curve. From this fit the dielectric constant and the thickness of the silver film were determined to be $\epsilon_3=-10.17+i0.348$ and $d_3=599$ Å. These values are consistent with the earlier data obtained for similar films. Here, again, the thickness of the MgF_2 film does not enter the fitting procedure because of index matching with the liquid. The dashed curve for the Raman-intensity variation was calculated using the above silver parameters in Eq. (A19). As we explained earlier, T of Eq. (A19) is proportional to the local light intensity at the outer surface of the silver film when a radiation of unit field strength is incident from the prism side. The dashed curve is a plot of T as a function of the incident angle. Although there is a slight disagreement on the high-angle side of the maximum, the Raman-intensity data (open circles) and the incident-intensity curve (dashed curve) agree remarkably well.

Figure 6 shows the corresponding data for the scattering angle. The Stokes-scattered light emerges with a wavelength at 6059 Å, so the ATR curve was also measured at the same wavelength produced by a dye laser. The theoretical curve for the ATR data (solid line) was obtained with $\epsilon_1=\epsilon_2=1.870$, $\epsilon_4=2.620$, $d_3=599$ Å, and $\epsilon_3=-15.80+i0.590$. These are reasonable values for the parameters at 6059 Å; in particular, the value of ϵ_3 is in good agreement with the value given by Johnson and Christy[9] for silver. The dashed curve representing the angular dependence of the emission intensity through the prism was calculated by using the above parameters in Eq. (A19). We see that the agreement between theory and experiment is excellent. To our knowledge the results shown in Figs. 5 and 6 represent the first unambiguous demonstration of the relation between the ATR spectra and the Raman scattering mediated by SPP's.

Figure 7 shows the Raman spectra of the 2930-cm^{-1} line of acetone measured from the different regions of the sample described in Fig. 1 and Table I. We recall that the different regions have different thicknesses of MgF_2 coating over the silver film. For this series of measurements both the incident and scattering angles were set at the peak positions determined by the preceding experiment, and the sample cell was filled with the index-matched liquid. As before, the incident light was p-polarized with the wavelength at 5145 Å, and the power was approximately 28 mW. As expected, the Raman intensity decreases with increasing thickness of the MgF_2 spacer layer. A semilogarithmic plot of the normalized peak intensity versus the spacer thickness is shown in Fig. 8. The straight line was found by the least-squares-fitting procedure, and the equation for this line is given by

$$\ln\left[\frac{I(\theta_i,\theta_s,d_2)}{I(\theta_i,\theta_s,0)}\right]=0.346(\pm0.003)-2.601(\pm0.057)\times10^{-3}d_2(\text{Å})\,. \quad (3)$$

From Eq. (1) we have

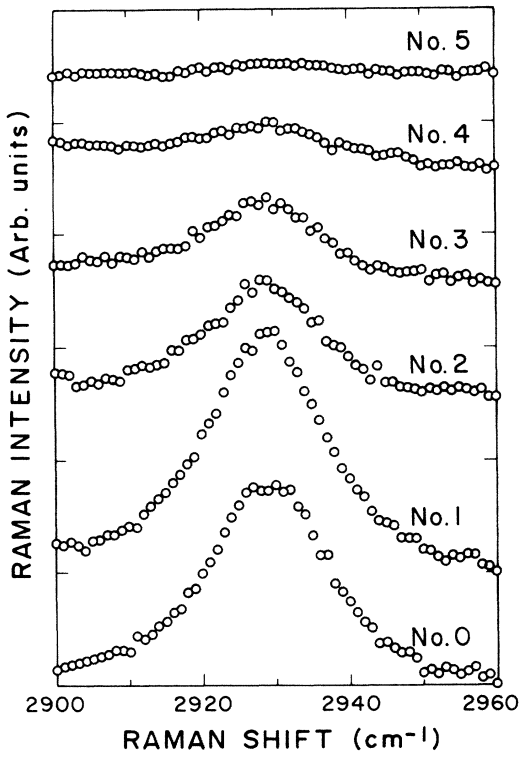

FIG. 7. Raman spectra for the six different sample regions with different MgF_2 spacer thicknesses.

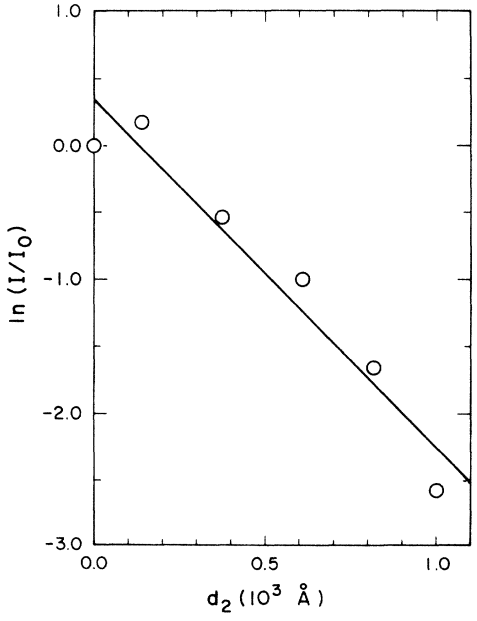

FIG. 8. Semilogarithmic plot of the normalized Raman intensity as a function of spacer thickness d_2.

$$\ln\left[\frac{I(\theta_i,\theta_s,d_2)}{I(\theta_i,\theta_s,0)}\right]\equiv -4\alpha d_2 , \tag{4}$$

where α is the effective decay constant of the field amplitude given by the decay constants at the incident- and scattered-light frequencies:

$$\alpha=-\frac{i}{2}[k_z(1,\omega_i)+k_z(1,\omega_s)] . \tag{5}$$

The constant term in Eq. (3) is nonzero, because the value for $I(\theta_i,\theta_s,0)$ corresponding to the bare part of the silver film is affected by an irregular behavior of the bare film under laser irradiation, as we have discussed before. From the slope of Eqs. (3) and (4) with respect to d_2, we obtain

$$l_d=\frac{1}{\alpha}=1539\pm 33\ \text{Å} .$$

This is the effective penetration depth of the SPP field into the liquid, and determines the layer thickness that is sampled by Raman scattering. When we calculate this length from the previously determined values of the dielectric constants at 5145 and 6059 Å, we obtain the value 1534 Å; this is remarkably close to the above experimental value.

IV. DISCUSSION AND CONCLUSION

The most important result of the present work is that we were able to measure the decay length of SPP's outside the silver film directly. This was made possible by the use of an index-matched liquid as the Raman scattering medium. The precise agreement we found between the measured value of $l_d=1539\pm 33$ Å and the calculated value of 1534 Å is an indication of the accuracy of the theory as well as the precision of the dielectric parameters that enter the calculation. We believe that this is the first time that the decay length of SPP's has been measured directly in the optical frequency. Since the only ingredients of the theory are the Maxwell equations and the boundary conditions, it is not surprising that the theory predicts the measured results accurately. Nevertheless, it is gratifying to find that the macroscopic theory works accurately even when the thicknesses of the layers are much smaller than the wavelength of the light. We have earlier shown that the ATR method is sensitive enough to detect a submonolayer of adsorbed molecules on a silver surface.[10] The present result adds further confidence to the accuracy of the ATR method and Raman scattering involving almost microscopic distances near interfaces.

In the process of evaluating the dielectric constant of silver films in contact with air, MgF_2, and the liquid mixture, we have confirmed the result reported by Gugger *et al.*[8] that the dielectric constant of thin metal films depends on the dielectric constant of the adjacent medium. We found that the so-called "index-of-refraction–induced change" in the dielectric constant of silver can be accounted for by assuming the presence of a very thin (10 Å) transition layer between the silver film and air. One must be careful to limit the incident laser power in making ATR measurements, because an exposure to strong light

in the presence of a liquid changes the surface properties of silver.

By making ATR measurements and Raman measurements on a single sample *in situ*, we have demonstrated clearly that the maximum in the Raman intensity as a function of the incident angle is due to resonant enhancement of SPP's, which corresponds to the dip in the ATR spectrum. The scattered light can also couple resonantly with SPP's and produce a maximum in the Raman intensity as a function of the scattering angle. We have shown that the angle dependence of the Raman intensity, on both the incident angle and scattering angles, can be accurately predicted from the data obtained by ATR measurements. Thus, we can say that we understand this Raman-enhancement process completely now.

ACKNOWLEDGMENTS

This research was supported in part by the U.S. Department of Energy under Contract No. DE-FG03-85ER45196 and by the U.S. National Aeronautics and Space Administration under Grant No. NAG-524. We thank these agencies for their support of this research. One of us (J.C.H.) acknowledges partial support by the Alfred P. Sloan Foundation.

APPENDIX

The purpose of this appendix is to present an outline of the derivation of the expressions for the reflectivity and the surface polariton dispersion relation for an n-layered structure shown in Fig. 9. In this process we will clarify the apparent inconsistencies between the equations that appeared in the earlier papers our group has published.[10,11] The method outlined here has been used by a number of authors including Abelès,[12] Born and Wolf,[13] Heavens,[14] and Sipe.[15] Reference 11 contains an essentially parallel discussion of this method to the present one, but we present a more complete analysis here.

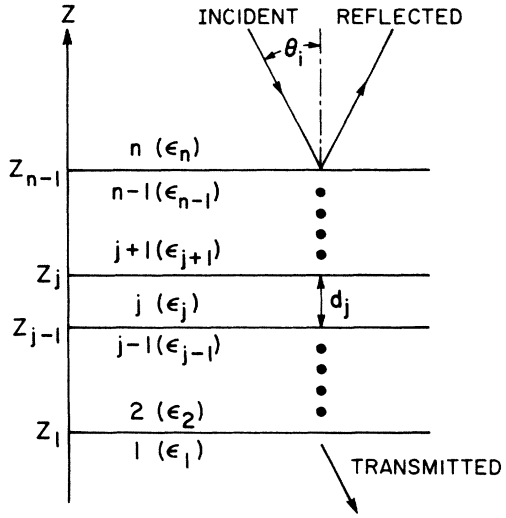

FIG. 9. Definition of parameters for an n-layered geometry.

Let us consider the electromagnetic waves that propagate in an n-layered structure shown in Fig. 9. The layers are stacked along the z direction and have infinite extent in the x and y directions. Layer 1 and layer n extend to $z\rightarrow-\infty$ and $z\rightarrow+\infty$, respectively, and the intermediate layers are bounded at $z_1,z_2,\ldots,z_{n-1}$. The dielectric constant of each layer is designated by $\epsilon(1),\epsilon(2),\ldots,\epsilon(n)$, and the thickness of the jth layer is given by

$$d_j=z_j-z_{j-1} \quad \text{for } 2\leq j\leq n-1 . \tag{A1}$$

Since we assume that the dielectrics or metals that form the n layers are uniform and isotropic, without loss of generality we can assume that the surface polaritons (SP's) in this structure propagate along the x direction with a real wave vector $k_{||}$ along the interfaces. Then at frequency ω, the form of the electric field in layer j can be written as

$$\mathbf{E}(j)=[\mathbf{A}(j)e^{ik_z(j)(z-z_{j-1})}+\mathbf{B}(j)e^{-ik_z(j)(z-z_{j-1})}]e^{i(k_{||}x-\omega t)} , \tag{A2}$$

where the wave-vector component along the z direction, $k_z(j)$, is given by

$$k_z(j)=\left[\frac{\epsilon(j)\omega^2}{c^2}-k_{||}^2\right]^{1/2} , \tag{A3}$$

and c is the speed of light in vacuum. $\mathbf{A}(j)$ and $\mathbf{B}(j)$ are the field amplitude vectors with the three components $A_\mu(j)$ and $B_\mu(j)$ for $\mu=x,y,z$. The relations among $A_\mu(j)$ and $B_\mu(j)$ are determined by the requirement that they satisfy the Maxwell equations and the boundary conditions at the $n-1$ interfaces at $z_1,z_2,\ldots,z_{n-1}$.

Matching the boundary conditions at $z=z_j$ for p-polarized [transverse magnetic (TM)] light yields the result

$$\begin{bmatrix}A_x(j+1)\\B_x(j+1)\end{bmatrix}=\underline{M}_{\mathrm{TM}}(j+1,j)\begin{bmatrix}A_x(j)\\B_x(j)\end{bmatrix} , \tag{A4}$$

where $\underline{M}_{\mathrm{TM}}(j+1,j)$ is a matrix given by

$$\underline{M}_{\mathrm{TM}}(j+1,j)=\frac{1}{2}\begin{bmatrix}\left[1+\frac{\epsilon(j)k_z(j+1)}{\epsilon(j+1)k_z(j)}\right]e^{ik_z(j)d_j} & \left[1-\frac{\epsilon(j)k_z(j+1)}{\epsilon(j+1)k_z(j)}\right]e^{-ik_z(j)d_j}\\ \left[1-\frac{\epsilon(j)k_z(j+1)}{\epsilon(j+1)k_z(j)}\right]e^{ik_z(j)d_j} & \left[1+\frac{\epsilon(j)k_z(j+1)}{\epsilon(j+1)k_z(j)}\right]e^{-ik_z(j)d_j}\end{bmatrix} . \tag{A5}$$

Then it follows that

$$\begin{bmatrix} A_x(l) \\ B_x(l) \end{bmatrix} = \left[\prod_{j=k}^{l-1} \underline{M}_{\mathrm{TM}}(j+1,j) \right] \begin{bmatrix} A_x(k) \\ B_x(k) \end{bmatrix} \tag{A6}$$

for $l \geq k+1$. For p-polarized light, $A_y(j)=B_y(j)=0$ and

$$A_z(j) = -\frac{k_{||}}{k_z(j)} A_x(j) , \tag{A7}$$

$$B_z(j) = \frac{k_{||}}{k_z(j)} B_x(j) \tag{A8}$$

from the Maxwell equations. Thus, knowledge of $A_x(j)$ and $B_x(j)$ is sufficient to determine the complete electric field in layer j.

For s-polarized light (transverse electric) the expression corresponding to Eq. (A4) reads

$$\begin{bmatrix} A_y(j+1) \\ B_y(j+1) \end{bmatrix} = \frac{1}{2} \begin{bmatrix} \left[1+\frac{k_z(j)}{k_z(j+1)}\right] e^{ik_z(j)d_j} & \left[1-\frac{k_z(j)}{k_z(j+1)}\right] e^{-ik_z(j)d_j} \\ \left[1-\frac{k_z(j)}{k_z(j+1)}\right] e^{ik_z(j)d_j} & \left[1+\frac{k_z(j)}{k_z(j+1)}\right] e^{-ik_z(j)d_j} \end{bmatrix} \begin{bmatrix} A_y(j) \\ B_y(j) \end{bmatrix} , \tag{A9}$$

and $A_x(j)=A_z(j)=B_x(j)=B_z(j)=0$.

To obtain the expression for the reflectivity and the dispersion relation for surface polaritons in the structure, it is convenient to define a matrix $\underline{M}_{\mathrm{TM}}$ by

$$\underline{M}_{\mathrm{TM}} \equiv \prod_{j=1}^{n-1} \underline{M}_{\mathrm{TM}}(j+1,j) \equiv \begin{bmatrix} M_{11} M_{12} \\ M_{21} M_{22} \end{bmatrix} . \tag{A10}$$

Then,

$$\begin{bmatrix} A_x(n) \\ B_x(n) \end{bmatrix} = \underline{M}_{\mathrm{TM}} \begin{bmatrix} A_x(1) \\ B_x(1) \end{bmatrix} . \tag{A11}$$

At this point it is useful to go back to Eq. (A3) and establish a consistent sign convention in taking the square root. Since we assume that ω and $k_{||}$ are real, and $\mathrm{Im}\epsilon(j)>0$,[16] $\mathrm{Im}k_z^2(j)>0$ and $k_z^2(j)$ lie in the upper half of the complex plane. It follows that $k_z(j)$ lies either in the first quadrant [$\mathrm{Re}k_z(j)>0$ and $\mathrm{Im}k_z(j)>0$] or in the third quadrant [$\mathrm{Re}k_z(j)<0$ and $\mathrm{Im}k_z(j)<0$] of the complex plane. We take the square root in Eq. (A3) so that $k_z(j)$ lies in the first quadrant:

$$\mathrm{Re}k_z(j)>0 \quad \text{and} \quad \mathrm{Im}k_z(j)>0 . \tag{A12}$$

Then by reference to Eq. (A2), we see that $\mathbf{A}(j)$ represents a wave propagating in the positive z direction and $\mathbf{B}(j)$ represents a wave propagating in the negative z direction. Thus the reflectivity of the dielectric stack when the incident and reflected light is in medium n and p-polarized is given by

$$R = \frac{|\hat{\mathbf{x}}A_x(n)+\hat{\mathbf{z}}A_z(n)|^2}{|\hat{\mathbf{x}}B_x(n)+\hat{\mathbf{z}}B_z(n)|^2} , \tag{A13}$$

with the condition that there is no upward propagating wave in medium 1, i.e.,

$$A_x(1)=A_z(1)=0 . \tag{A14}$$

By use of Eqs. (A7) and (A8), Eq. (A13) can be simplified to the form

$$R = \left| \frac{A_x(n)}{B_x(n)} \right|^2 . \tag{A15}$$

From Eqs. (A11) and (A14) we have

$$\begin{bmatrix} A_x(n) \\ B_x(n) \end{bmatrix} = \begin{bmatrix} M_{11} & M_{12} \\ M_{21} & M_{22} \end{bmatrix} \begin{bmatrix} 0 \\ B_x(1) \end{bmatrix} = \begin{bmatrix} M_{12} \\ M_{22} \end{bmatrix} B_x(1) . \tag{A16}$$

Therefore,

$$R = \left| \frac{M_{12}}{M_{22}} \right|^2 . \tag{A17}$$

By similar reasoning, the same form is obtained for the reflectivity of s-polarized light incident in medium n.

Next, we define the transmissivity of the stack T for p-polarized light as the ratio of the intensity of the transmitted light at $z=z_1$ to the incident intensity in medium n at $z=z_{n-1}$, that is,

$$T = \left| \frac{\hat{\mathbf{x}}B_x(1)+\hat{\mathbf{z}}B_z(1)}{\hat{\mathbf{x}}B_x(n)+\hat{\mathbf{z}}B_z(n)} \right|^2 . \tag{A18}$$

Again we have assumed that there is no upward propagating wave in medium 1, i.e., Eq. (A14). By use of Eqs. (A8) and (A16), this expression can be simplified to the form

$$T = \frac{1}{|M_{22}|^2} \left[\cos^2\theta + \left| \frac{k_z(n)}{k_z(1)} \right|^2 \sin^2\theta \right] , \tag{A19}$$

where θ is the angle of incidence in medium n and we have used the relation $k_{||}/k_z(n)=\tan\theta$.

The dispersion relation for SP's in the layered structure is obtained by requiring that the fields remain finite as $z\rightarrow\pm\infty$. Since $\mathrm{Im}k_z(j)>0$ for $j=1$ and n in particular, by reference to Eq. (A2) this requirement is

$$B_x(n)=A_x(1)=0 . \tag{A20}$$

Thus,

$$\begin{bmatrix} A_x(n) \\ 0 \end{bmatrix} = \begin{bmatrix} M_{11} & M_{12} \\ M_{21} & M_{22} \end{bmatrix} \begin{bmatrix} 0 \\ B_x(1) \end{bmatrix} = \begin{bmatrix} M_{12} \\ M_{22} \end{bmatrix} B_x(1) ,$$

and, therefore, the dispersion relation is

$$M_{22}=0 . \tag{A21}$$

Equations (A17) and (A19) are the final results we use in our analysis of data, and this completes the outline of the matrix method applied to our geometry.

Now let us examine the equations presented earlier by our group[10,11] and clarify their relations to the present results. Equation (3) of Ref. 11 is obtained by making a replacement $ik_z(j)\rightarrow\alpha_j$. There the sign convention in taking the square root in the expression corresponding to Eq. (A3) was $\mathrm{Re}\alpha_j\geq 0$, and when $\mathrm{Re}\alpha_j=0$, then $\mathrm{Im}\alpha_j\leq 0$. This convention corresponds to using the third quadrant in k_z space, i.e., $\mathrm{Re}k_z(j)<0$ and $\mathrm{Im}k_z(j)<0$ in the present notation. Under this sign convention the propagation directions for A and B terms in Eq. (A2) get reversed, and the matrix elements of Eqs. (A5) and (A10) are transformed according to the rule $M_{11}\rightleftarrows M_{22}$ and $M_{21}\rightleftarrows M_{12}$. Thus the expressions for reflectivity and the dispersion relation transform to

$$R=\left|\frac{M_{21}}{M_{11}}\right|^2 \quad \text{and} \quad M_{11}=0 ,$$

respectively, as given in Eq. (7) and just below that in Ref. 11.

In Ref. 10 the reflectivity expression was considered for incidence angles $\phi_i>\phi_c$, where ϕ_c is the critical angle for the prism given by

$$\sin\phi_c=\frac{1}{\sqrt{\epsilon(n)}}\equiv\frac{1}{(\epsilon_p)^{1/2}} .$$

For this case, $\alpha_3\equiv ik_z(3)$ is pure imaginary and $\alpha_1\equiv ik_z(1)$ in vacuum is pure real. The choice of signs used in taking the square root in the expression $\alpha_j=(k_{||}^2-\epsilon_j\omega^2/c^2)^{1/2}$ in that paper was that

$$\mathrm{Re}\alpha_1>0 \quad \text{and} \quad \mathrm{Im}\alpha_0=0 ,$$

and

$$\mathrm{Re}\alpha_2\geq 0 ,$$

and if

$$\mathrm{Re}\alpha_2=0 ,$$

then

$$\mathrm{Im}\alpha_2\leq 0 ,$$

and

$$\mathrm{Re}\alpha_3=0, \quad \mathrm{Im}\alpha_3>0 .$$

In terms of $k_z(j)$ used in this appendix, this translates into

$$\mathrm{Re}k_z(1)=0 \quad \text{and} \quad \mathrm{Im}k_z(1)<0 ,$$

and

$$\mathrm{Im}k_z(2)\leq 0 ,$$

and if

$$\mathrm{Im}k_z(2)=0 ,$$

then

$$\mathrm{Re}k_z(2)\leq 0 ,$$

and

$$\mathrm{Re}k_z(3)>0, \quad \mathrm{Im}k_z(3)=0 .$$

When we compare this sign convention with the one we have adopted here, Eq. (A12), we see that we must make the following transformations in Eq. (A5): $k_z(1)\rightarrow -k_z(1)$, $k_z(2)\rightarrow -k_z(2)$, and $k_z(3)\rightarrow k_z(3)$. When we apply this change of signs to the matrix elements of Eq. (A5), the net result is a transformation of the matrix elements of Eq. (A10) according to the rule $M_{12}\rightleftarrows M_{11}$ and $M_{22}\rightleftarrows M_{21}$. Thus the reflectivity under the sign convention used in Ref. 10 is given by

$$R=\left|\frac{M_{11}}{M_{21}}\right|^2 ,$$

as given in Eq. (5) in Ref. 10. [There is a typographical error in the denominator of Eq. (5), and m_{21} should have been printed in place of m_{12}.]

The dispersion relation given in Ref. 10 ($M_{11}=0$) was a result from yet another sign convention, namely $\mathrm{Re}\alpha_j>0$ for all j. This choice implies $\mathrm{Im}k_z(j)<0$ and, consequently, we must have $\mathrm{Re}k_z(j)<0$, because $k_z(j)$ can lie only in the first or third quadrant. Then, as we have seen before in examining the sign convention of Ref. 11, the matrix matrix elements of Eq. (A10) become diagonally interchanged, and thus the dispersion relation is given by $M_{11}=0$.

This completes the clarification of apparently different expressions for the reflectivity and the dispersion relation published previously by our group. It was unfortunate that casual choices of signs were made earlier and different looking expressions have been presented. However, we emphasize here that the formulas used in the numerical computation contained internally consistent sign conventions and the numerical results reported in Refs. 10 and 11 are correct.

*Permanent address: Department of Electronics, University of Osaka Prefecture, Sakai, Osaka 591, Japan.

†Present address: Research Institute of Electrical Communication, Tohoku University, Sendai 980, Japan.

[1]Y. Y. Chen, W. P. Chen, and E. Burstein, Phys. Rev. Lett. **36**, 1207 (1976); Bull. Am. Phys. Soc. **21**, 338 (1976).

[2]K. Sakoda, K. Ohtaka, and E. Hanamura, Solid State Commun. **41**, 393 (1982).

[3]S. Ushioda and Y. Sasaki, Phys. Rev. B **27**, 1401 (1983).

[4]B. Pettinger, A. Tadjeddine, and D. M. Kolb, Chem. Phys. Lett. **66**, 544 (1976).

[5]J. C. Tsang, J. R. Kirtley, and T. N. Theis, Solid State Commun. **35**, 667 (1980).

[6]C. K. Chen, A. R. B. de Castro, Y. R. Shen, and F. De Martini, Phys. Rev. Lett. **43**, 946 (1979).

[7]C. E. Reed, Ph.D. thesis, University of California, Irvine, 1986.

[8]H. Gugger, M. Jurich, J. D. Swalen, and A. J. Sievers, Phys. Rev. B **30**, 4189 (1984).

[9]P. B. Johnson and R. W. Christy, Phys. Rev. B **6**, 4370 (1972).

[10]J. Giergiel, C. E. Reed, S. Ushioda, and J. C. Hemminger, Phys. Rev. B **31**, 3323 (1985).

[11]C. E. Reed, J. Giergiel, S. Ushioda, and J. C. Hemminger, Phys. Rev. B **31**, 1873 (1985).

[12]F. Abelès, Ann. Phys. (Paris) **3**, 504 (1948); **5**, 596 (1950); **5**, 706 (1950).

[13]M. Born and E. Wolf, *Principles of Optics* (Pergamon, Oxford, 1975), pp. 51–70 and 627–633.

[14]O. S. Heavens, *Optical Properties of Thin Solid Films* (Dover, New York, 1965), pp. 69–80.

[15]J. E. Sipe, Surf. Sci. **105**, 489 (1981).

[16]$\mathrm{Im}\epsilon(j) > 0$ for all media, except when there is population inversion, as in a lasing medium. In vacuum, $\mathrm{Im}\epsilon(\mathrm{vac}) = 0$, but we will keep a positive infinitesimal imaginary part to avoid k_z on the imaginary axis, where the propagation direction cannot be defined.